REMUNOM
ISSN 2178-6925

Received: 10/11/2026 - **Accepted:** 15/11/2026
Vol: 13.24
DOI: 10.66104/vhwccn53
Pages: 1-24

CARACTERIZAÇÃO INTEGRADA DE UM MINÉRIO DE COBRE: CARACTERÍSTICAS QUÍMICAS, MINERALÓGICAS, TÉRMICAS E MICROESTRUTURAIS E SUAS IMPLICAÇÕES PARA O BENEFICIAMENTO MINERAL

INTEGRATED CHARACTERIZATION OF A COPPER ORE: CHEMICAL, MINERALOGICAL, THERMAL, AND MICROSTRUCTURAL FEATURES AND THEIR IMPLICATIONS FOR MINERAL PROCESSING

CARACTERIZACIÓN INTEGRADA DE UN MINERAL DE COBRE: CARACTERÍSTICAS QUÍMICAS, MINERALÓGICAS, TÉRMICAS Y MICROESTRUCTURALES Y SUS IMPLICACIONES PARA EL PROCESAMIENTO DE MINERALES

Marcos Leandro dos Santos Boldrin
Graduando em Engenharia de Minas, Universidade Federal de Alfenas, Brazil
E-mail: marcos.boldrin@sou.unifal-mg.edu.br

Gabriel Mateus Oliveira Cubi
Mestre em Engenharia Química, Universidade Federal de Alfenas, Brazil
E-mail: gabriel.cubi@sou.unifal-mg.edu.br

Resumo

A relevância tecnológica da caracterização de minérios de cobre depende da interpretação conjunta da composição química, da assembleia mineral e das texturas das partículas. Este estudo integra fluorescência de raios X, difração de raios X, espectroscopia no infravermelho por transformada de Fourier, termogravimetria acoplada à calorimetria exploratória diferencial e microscopia eletrônica de varredura para caracterizar um minério de cobre e examinar suas implicações para o processamento mineral. A composição química foi dominada por SiO_2 (49,23% em massa), Fe_2O_3 equivalente (21,22%) e Al_2O_3 (9,87%), com 2,68% de CuO equivalente, correspondentes estequiometricamente a aproximadamente 2,14% de Cu. A assembleia cristalina identificada compreendeu quartzo, clorita,

CC BY

REMUNOM
ISSN 2178-6925

Received: 10/11/2026 - **Accepted:** 15/11/2026
Vol: 13.24
DOI: 10.66104/vhwccn53
Pages: 1-24

anfibólio, feldspatos, magnetita, calcopirita e apatita. A absorção no infravermelho associada às vibrações dos silicatos e aos componentes hidroxilados complementou as evidências de difração. A curva termogravimétrica indicou perda líquida de massa de aproximadamente 2,3% a 1000 °C, com a principal redução em temperaturas elevadas, compatível com contribuições de minerais hidratados, mas insuficiente para atribuir individualmente as reações. As imagens de elétrons retroespalhados mostraram partículas angulosas, domínios internos contrastantes e texturas compostas, sem fornecer liberação mineral quantitativa ou identificação de fases em partículas específicas. As evidências destacam a relevância da exposição mineral, da rejeição de silicatos e do possível arraste de clorita para investigações de flotação. Também apontam a reatividade da ganga e a acessibilidade do cobre como aspectos importantes para estudos de lixiviação. Os resultados fundamentam ensaios posteriores de beneficiamento, distinguindo características observadas de desempenhos metalúrgicos ainda não verificados.

Palavras-chave: Minério de cobre; Caracterização integrada; Mineralogia da ganga; Associações minerais; Processamento mineral.

Abstract

The technological significance of copper ore characterization depends on how chemical composition, mineral assemblages and particle textures are interpreted jointly. This study integrates X-ray fluorescence, X-ray diffraction, Fourier-transform infrared spectroscopy, thermogravimetry coupled with differential scanning calorimetry, and scanning electron microscopy to characterize a copper ore and examine its implications for mineral processing. The chemical composition was dominated by SiO_2 (49.23 wt.%), Fe_2O_3 equivalent (21.22 wt.%) and Al_2O_3 (9.87 wt.%), with 2.68 wt.% CuO equivalent, corresponding stoichiometrically to approximately 2.14 wt.% Cu. The identified crystalline assemblage comprised quartz, chlorite, amphibole, feldspars, magnetite, chalcopyrite and apatite. Infrared absorption associated with silicate vibrations and hydroxyl-bearing components complemented the diffraction evidence. The thermogravimetric curve indicated a net mass loss of approximately 2.3% at 1000 °C, with the principal decrease occurring at elevated temperatures, consistent with contributions from hydrous minerals but insufficient for assigning individual reactions uniquely. Backscattered-electron images showed angular particles, contrasting internal domains and composite textures, without providing quantitative mineral liberation or particle-specific phase identification. The combined evidence highlights the relevance of mineral exposure, silicate rejection and potential chlorite entrainment for flotation investigations. It also identifies gangue reactivity and copper accessibility as important considerations for leaching studies. These findings establish an experimentally grounded basis for subsequent processing tests while distinguishing observed material characteristics from unverified metallurgical performance.

Keywords: Copper ore; Integrated characterization; Gangue mineralogy; Mineral associations; Mineral processing.

CC BY

REMUNOM
ISSN 2178-6925

Received: 10/11/2026 - **Accepted:** 15/11/2026
Vol: 13.24
DOI: 10.66104/vhwccn53
Pages: 1-24

Resumen

La relevancia tecnológica de la caracterización de minerales de cobre depende de la interpretación conjunta de la composición química, la asociación mineral y las texturas de las partículas. Este estudio integra fluorescencia de rayos X, difracción de rayos X, espectroscopia infrarroja por transformada de Fourier, termogravimetría acoplada con calorimetría diferencial de barrido y microscopía electrónica de barrido para caracterizar una mena de cobre y examinar sus implicaciones para el procesamiento mineral. La composición química estuvo dominada por SiO_2 (49,23% en masa), Fe_2O_3 equivalente (21,22%) y Al_2O_3 (9,87%), con 2,68% de CuO equivalente, correspondientes estequiométricamente a aproximadamente 2,14% de Cu. La asociación cristalina identificada comprendió cuarzo, clorita, anfíbol, feldespatos, magnetita, calcopirita y apatita. La absorción infrarroja asociada con las vibraciones de los silicatos y los componentes hidroxilados complementó las evidencias de difracción. La curva termogravimétrica indicó una pérdida neta de masa de aproximadamente 2,3% a 1000 °C, con la principal disminución a temperaturas elevadas, compatible con contribuciones de minerales hidratados, pero insuficiente para asignar individualmente las reacciones. Las imágenes de electrones retrodispersados mostraron partículas angulosas, dominios internos contrastantes y texturas compuestas, sin proporcionar liberación mineral cuantitativa ni identificación de fases en partículas específicas. Las evidencias destacan la relevancia de la exposición mineral, el rechazo de silicatos y el posible arrastre de clorita para investigaciones de flotación. También señalan la reactividad de la ganga y la accesibilidad del cobre como aspectos importantes para estudios de lixiviación. Los resultados fundamentan ensayos posteriores de beneficio, distinguiendo características observadas de desempeños metalúrgicos todavía no verificados.

Palabras clave: Mena de cobre; Caracterización integrada; Mineralogía de ganga; Asociaciones minerales; Procesamiento mineral.

1. Introduction

Copper recovery from an ore depends on the minerals that host the metal and on their relationships with the surrounding gangue. A bulk chemical assay establishes the amount of copper in the analyzed material, but it does not reveal whether the copper-bearing grains are exposed, enclosed in silicates or distributed among phases with different surface and dissolution properties. These distinctions affect the amount of grinding required, the separation of valuable particles from gangue, and the accessibility of copper to leaching solutions. Studies coupling quantitative mineralogy with flotation have demonstrated that mineral associations

CC BY

REMUNOM
ISSN 2178-6925

Received: 10/11/2026 - **Accepted:** 15/11/2026
Vol: 13.24
DOI: 10.66104/vhwccn53
Pages: 1-24

and feed variability contribute to differences in recovery and concentrate quality even within a single deposit (Tijsseling et al., 2020; Shi et al., 2025).

The gangue assemblage is particularly important in ores containing both framework silicates and hydrous silicates. Quartz, feldspars and chlorite cannot be treated as a single inert diluent when interpreting processing behavior. Their different structures and surface properties can affect fragmentation, particle interactions and reagent demand. Experiments with chlorite-containing systems have shown that gangue recovery can involve both surface-mediated flotation and mechanical entrainment, with particle size influencing the relative importance of these mechanisms (Pan et al., 2019; Chen et al., 2023). Consequently, a high bulk silica content alone provides insufficient information to anticipate flotation selectivity or pulp behavior.

Mineralogy also affects comminution and hydrometallurgy through mechanisms that are not captured by the total copper grade. Rincon et al. (2019) related comminution indices to mineralogical features in a copper ore, demonstrating the value of considering composition alongside measured breakage response. In leaching, the mineral species hosting Ca, Mg, Al and Fe govern their dissolution behavior and contribution to acid consumption. Thomas (2021) showed that gangue acid demand reflects the interplay of mineral dissolution and secondary precipitation. Such findings support the use of characterization to identify the variables that require testing, while avoiding direct predictions of energy consumption or extraction from chemical composition alone.

A complementary set of analytical techniques can resolve different parts of this problem. X-ray fluorescence (XRF) establishes bulk composition, whereas X-ray diffraction (XRD) identifies crystalline phases. Fourier-transform infrared spectroscopy (FTIR) provides information on vibrational groups, including silicate frameworks, hydroxyls and molecular water. Dehaine et al. (2022) demonstrated the geometallurgical usefulness of FTIR for Cu–Co ores when spectra were calibrated against quantitative mineralogical measurements. Without such calibration, FTIR remains valuable as complementary evidence, but absorption intensity cannot be directly translated into mineral abundance.

CC BY

REMUNOM
ISSN 2178-6925

Received: 10/11/2026 - **Accepted:** 15/11/2026
Vol: 13.24
DOI: 10.66104/vhwccn53
Pages: 1-24

Thermogravimetry and differential scanning calorimetry (TG–DSC) add information on mass changes and thermal events that may involve dehydration, dehydroxylation, oxidation and structural transformations. Interpretation in a multicomponent ore requires particular care because several processes can occur simultaneously. Studies of chlorites show that dehydroxylation and oxidation-related hydrogen release depend on composition and experimental conditions (Lempart et al., 2018; Lempart et al., 2020). Scanning electron microscopy (SEM), in turn, reveals particle morphology and spatial contrasts that bulk methods average out. Quantitative liberation analysis requires mineral classification and representative particle measurements beyond the visual inspection of backscattered-electron images (Fandrich et al., 2007).

This study integrates chemical, mineralogical, thermal, and microstructural characterization to investigate the relationships between copper-bearing phases, silicate gangue, and particle-scale heterogeneity in a copper ore. By combining XRF, XRD, FTIR, TG–DSC, and SEM, the study seeks to identify the main mineralogical and textural characteristics relevant to copper exposure, gangue rejection, and subsequent mineral processing investigations.

2. Materials and Methods

A 10 kg sample of Brazilian copper ore, previously sampled by the supplying company, was received for chemical, mineralogical, thermal, and microstructural characterization. The material was initially crushed to 100% passing 3.35 mm, homogenized using an elongated pile procedure, and divided into analytical aliquots of 100 g. A portion was pulverized and sieved to obtain a particle size below 74 μm for X-ray fluorescence (XRF), X-ray diffraction (XRD), Fourier-transform infrared spectroscopy (FTIR), and thermogravimetric and differential scanning calorimetry (TG–DSC) analyses. Additional particles were selected for scanning electron microscopy (SEM).

Chemical composition was determined by XRF using a Bruker S8 Tiger spectrometer. Major elements were analyzed using fused beads prepared with

CC BY

REMUNOM
ISSN 2178-6925

Received: 10/11/2026 - **Accepted:** 15/11/2026
Vol: 13.24
DOI: 10.66104/vhwccn53
Pages: 1-24

lithium tetraborate as flux, whereas minor elements, such as Cu, were determined using pressed pellets. Loss on ignition (LOI) was determined at 1000 °C for 5 h. Elemental concentrations were expressed as oxide equivalents in wt.% (normalized to 100%).

Mineralogical characterization was performed using a Bruker D8 Discover X-ray diffractometer equipped with Cu Kα radiation (λ = 1.5406 Å). Diffraction patterns were collected over a 2θ range of 5 to 70°, with a step size of 0.02°. Crystalline phases were identified using Match! software and reference patterns from the Crystallography Open Database (COD). Mineralogical interpretation was qualitative, based on the identification and correspondence of characteristic diffraction peaks.

FTIR analysis was conducted using a Bruker Vertex 70 spectrometer equipped with a diamond attenuated total reflectance (ATR) accessory. Spectra were acquired over the wavenumber range of 400 to 4000 cm^{-1} and presented in transmittance mode. The spectral minima were evaluated to identify characteristic vibrational features associated with silicate structures, hydroxyl groups, and water-bearing components, complementing the mineralogical information obtained by XRD.

Thermal characterization was performed using a Netzsch STA 449 F3 Nevio simultaneous thermal analyzer. TG–DSC measurements were conducted using approximately 30 mg of sample in an alumina crucible, under an atmospheric air atmosphere, from 30 to 1000 °C at a heating rate of 10 °C min^{-1}. Thermogravimetric results were expressed as relative mass (%), while the DSC signal was recorded in mW mg^{-1}. The combined thermal curves were evaluated to identify mass changes and thermal events associated with transformations of the mineral constituents.

Microstructural characterization was performed by SEM using a TESCAN MIRA 4 LMU microscope at the Centro de Microscopia (CEMIC), Federal University of Alfenas (UNIFAL-MG), Brazil. The particles were embedded in resin, polished, and coated with a carbon layer prior to analysis. Backscattered-electron images were obtained using a low-energy backscattered-electron (LE-BSE) detector at an accelerating voltage of 20 kV and a working distance of 12.03 mm. The images

CC BY

REMUNOM
ISSN 2178-6925

Received: 10/11/2026 - **Accepted:** 15/11/2026
Vol: 13.24
DOI: 10.66104/vhwccn53
Pages: 1-24

were examined to evaluate particle morphology, compositional contrast, and textural relationships among mineral constituents.

3. Results and Discussion

3.1 Integrated characterization of the copper ore

The chemical composition of the copper ore is presented in Figure 1. SiO_2 was the predominant component (49.23 wt.%), followed by Fe_2O_3 (21.22 wt.%) and Al_2O_3 (9.87 wt.%). CaO and MgO accounted for 5.45 and 5.22 wt.%, respectively, while CuO represented 2.68 wt.%. Minor constituents contributed 4.33 wt.%, and the loss on ignition was 2.00 wt.%.

Figure 1. Bulk chemical composition of the copper ore expressed as oxide equivalents (wt.%), with loss on ignition (LOI) included separately. “Others” represents the combined minor constituents.

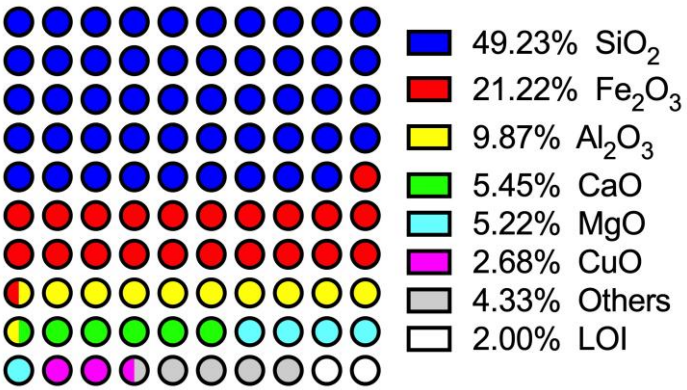

The silica and alumina contents together account for 59.10 wt.% of the reported composition, supporting the importance of a silicate-rich gangue. These oxide percentages cannot be interpreted as percentages of quartz and a discrete alumina phase. Silicon also occurs in feldspars, chlorite and amphibole, while aluminum can occupy structural sites in several of these minerals. Similarly, Fe expressed as Fe_2O_3 equivalent does not establish hematite as the iron-bearing phase. The reported form of the chemical analysis must therefore be distinguished from mineralogical identity before discussing beneficiation.

CC BY

REMUNOM
ISSN 2178-6925

Received: 10/11/2026 - **Accepted:** 15/11/2026
Vol: 13.24
DOI: 10.66104/vhwccn53
Pages: 1-24

The copper result requires the same distinction. A CuO-equivalent content of 2.68 wt.% corresponds to approximately 2.14 wt.% elemental Cu, calculated as 2.68 × 63.546/(63.546 + 15.999). The factor is approximately 0.799, and the conversion introduces no information about copper oxidation state, acid solubility or mineral distribution. In particular, the CuO label cannot be used as evidence that the ore is oxidized. The identification of a copper sulfide in the diffractogram provides the relevant mineralogical evidence, although qualitative XRD alone cannot establish what fraction of total copper resides in that sulfide.

The diffraction pattern identifies quartz, chlorite, amphibole, K-feldspar, plagioclase, magnetite, chalcopyrite and apatite (Figure 2). Quartz displays the most prominent reflection near 26.6° 2θ and additional labeled reflections near 20.9°, 36.5°, 39.5°, 40.3° and 50.1°. The recurrence of reflections at several positions is more informative than the tallest peak alone. Its strong intensity confirms that crystalline quartz is an important component of the pattern, but it does not establish quartz as 49.23 wt.% of the sample or provide a quantitative ranking against minerals with different diffraction responses.

Figure 2. X-ray diffraction pattern of the copper ore showing reflections assigned to quartz, chlorite, amphibole, K-feldspar, plagioclase, chalcopyrite, apatite, and magnetite.

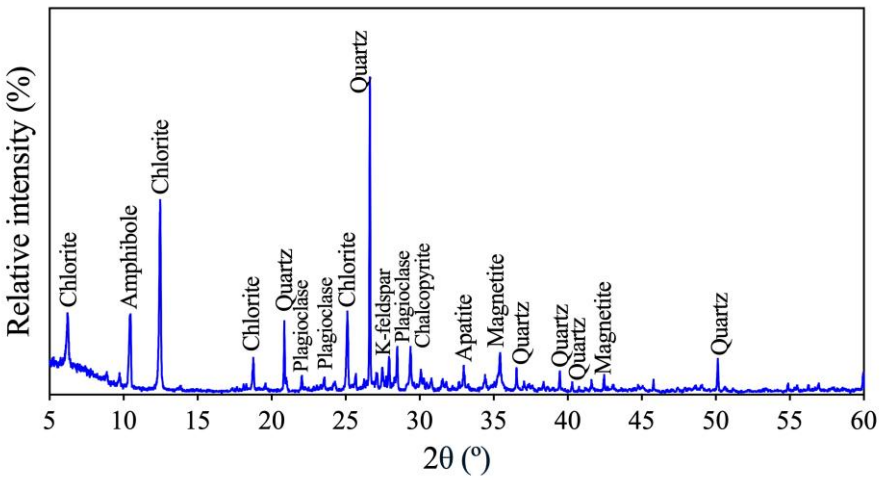

Low-angle reflections assigned to chlorite occur at approximately 6.2° and 12.4° 2θ, with further labeled features near 18.8° and 25.1°. Their association with

CC BY

REMUNOM
ISSN 2178-6925

Received: 10/11/2026 - **Accepted:** 15/11/2026
Vol: 13.24
DOI: 10.66104/vhwccn53
Pages: 1-24

the appreciable MgO, Al_2O_3 and iron contents is chemically coherent with an Fe–Mg-bearing phyllosilicate component. The amphibole assignment near 10.5° and the feldspar reflections in the approximately 22 to 29° region add plausible hosts for the remaining silicate-forming elements. These relationships support the combined assemblage without resolving chlorite composition, amphibole end member or plagioclase composition. Such distinctions would require more detailed diffraction evaluation and local chemical measurements.

Magnetite reflections labeled near 35.4° and 43° 2θ indicate the presence of a crystalline iron oxide, in addition to iron potentially hosted by silicate and sulfide phases. The reflection near 29.3° 2θ is consistent with chalcopyrite, although partial overlap with feldspar reflections may occur in this region. This assignment is further supported by the XRF results, which indicate 2.68 wt.% CuO equivalent, corresponding to approximately 2.14 wt.% elemental Cu. Moreover, no other crystalline Cu-bearing phases were identified in the diffraction pattern. The agreement between the chemical composition and the diffraction evidence therefore supports chalcopyrite as the principal identified copper-bearing mineral in the sample. Nevertheless, qualitative XRD cannot exclude the presence of minor or poorly crystalline Cu-bearing phases or establish the proportion of total copper hosted by chalcopyrite.

Apatite is labeled near 33° 2θ and provides a possible Ca-bearing accessory component, but its amount cannot be constrained from the CaO content. Calcium is also compatible with plagioclase and amphibole. The grouped “Others” category does not permit independent inspection of P, K, Na or S, so a complete element-to-mineral mass balance cannot be established. This is especially relevant for sulfur: a whole-rock sulfur determination would help constrain the sulfide inventory, whereas the present oxide-equivalent presentation cannot supply it by difference. The mineralogical interpretation is therefore consistent with the chemical results at the assemblage level, without becoming a quantitative allocation of each element.

FTIR adds evidence for a silicate framework and hydrogen-bearing components (Figure 3). The strongest broad absorption is located in the approximately 900 to 1150 cm^{-1} region, with a minimum near 1000 cm^{-1}. This

CC BY

REMUNOM
ISSN 2178-6925

Received: 10/11/2026 - **Accepted:** 15/11/2026
Vol: 13.24
DOI: 10.66104/vhwccn53
Pages: 1-24

envelope is compatible with overlapping Si–O stretching contributions from the identified silicates. Additional structure around approximately 700 to 800 cm^{-1} and strong absorption in the approximately 450 to 550 cm^{-1} region can include silicate framework and bending vibrations. Given the coexistence of quartz, feldspars, chlorite and amphibole, assigning every visible feature to one mineral would exceed the information provided by the bulk spectrum.

Figure 3. FTIR spectrum of the copper ore showing characteristic absorption bands associated with silicate vibrations and hydroxyl-bearing components.

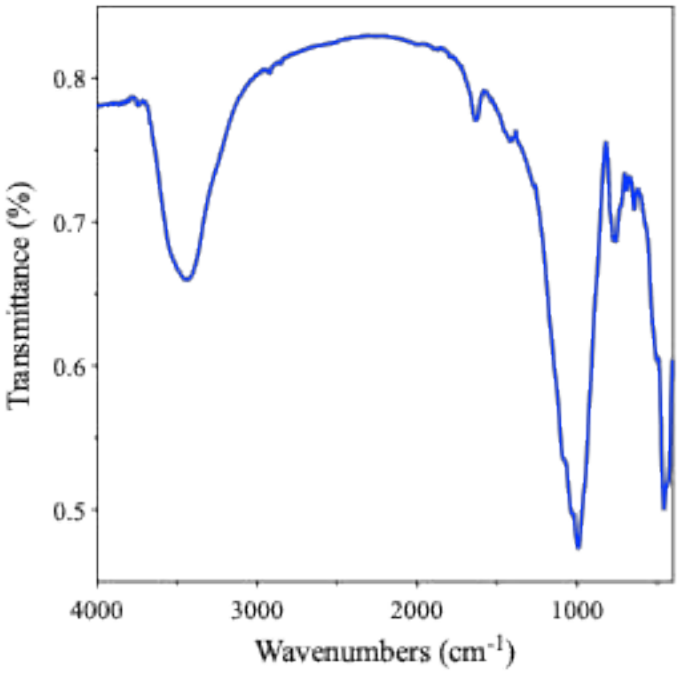

A broad high-wavenumber absorption centered approximately around 3400 to 3500 cm^{-1} and a smaller feature near 1640 cm^{-1} are consistent with hydrogen-bonded OH and molecular water contributions. Chlorite and amphibole provide mineralogical support for structural hydroxyls, but the broad high-wavenumber feature cannot be attributed entirely to one of these minerals. Adsorbed water and water associated with mineral surfaces may also contribute. Che et al. (2011) showed that the infrared response of phyllosilicates changes with dehydration and

CC BY

REMUNOM
ISSN 2178-6925

Received: 10/11/2026 - **Accepted:** 15/11/2026
Vol: 13.24
DOI: 10.66104/vhwccn53
Pages: 1-24

dehydroxylation and depends on mineral structure and octahedral cations. The present spectrum supports hydrogen-bearing components without resolving their relative proportions.

Quartz-rich material can also retain water and surface hydroxyl groups. Gaweł et al. (2020) demonstrated changes in these species during thermal, mechanical and chemical treatment of natural quartz. Consequently, the simultaneous presence of quartz reflections and OH-related absorption is not contradictory. For this sample, the most defensible interpretation combines structural OH in hydrous silicates with possible surface-associated water. The FTIR data do not establish a separate amorphous silica phase, nor do they justify assigning carbonate minerals solely from weak intermediate-wavenumber features that lack independent mineralogical confirmation.

The spectrum provides limited independent information on the copper-bearing fraction. Characterization of isolated chalcopyrite can combine vibrational and thermal measurements (Prameena et al., 2014), but a bulk spectrum dominated by silicates cannot be expected to isolate every sulfide contribution. The absence of a distinct copper-specific band therefore does not invalidate the chalcopyrite assignment in XRD. This illustrates the different analytical weighting of the two methods: a phase with a recognizable diffraction reflection can still make a small or unresolved contribution to an overlapping infrared envelope.

The TG curve remains close to its initial mass through much of the lower-temperature interval (Figure 4). A small initial decrease is followed by limited variation up to approximately 400 to 450 °C. A shallow rise is visible around approximately 450 to 520 °C, after which mass decreases progressively. The largest decrease occurs broadly between approximately 550 and 800 °C, followed by a slower decrease toward 1000 °C. The final mass is approximately 97.7% of the initial value, corresponding to a net loss of about 2.3%. These approximate values describe the plotted curve and should not be interpreted as independently resolved reaction boundaries.

Figure 4. TG–DSC curves of the copper ore recorded up to 1000 °C. The blue curve

CC BY

REMUNOM
ISSN 2178-6925

Received: 10/11/2026 - **Accepted:** 15/11/2026
Vol: 13.24
DOI: 10.66104/vhwccn53
Pages: 1-24

represents relative mass, while the red curve represents the DSC signal, with the exothermic direction indicated upward.

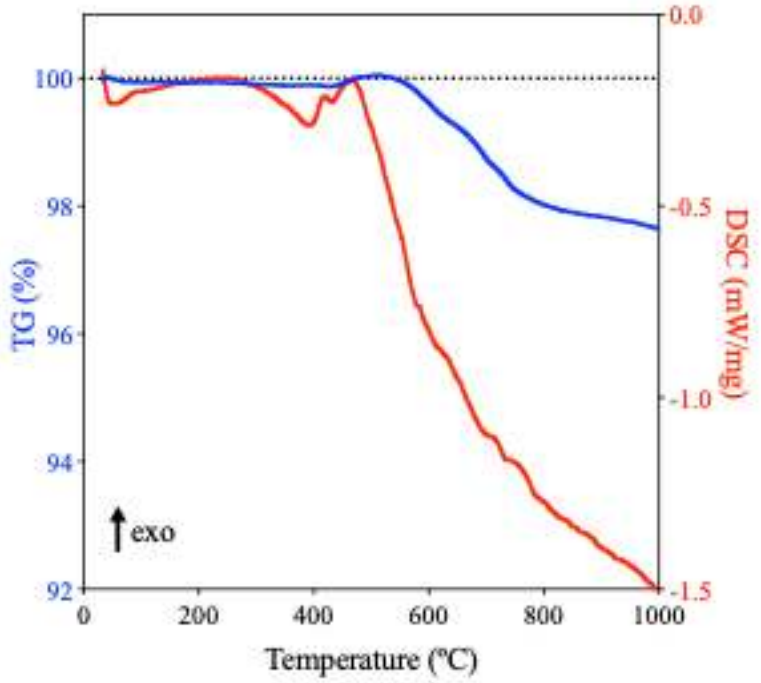

The elevated-temperature mass decrease is compatible with a contribution from dehydroxylation of the hydrous silicate fraction identified by XRD and supported by FTIR. However, chlorite thermal behavior cannot be reduced to a single water-release step. Lempart et al. (2018) demonstrated that Fe-bearing chlorites can undergo both dehydroxylation and dehydrogenation, including under an inert atmosphere. Their subsequent evolved-gas study showed that the relation between TG mass loss and released hydrogen-bearing species changes with atmosphere and Fe–Mg composition (Lempart et al., 2020). Thus, the measured net loss cannot be converted directly into chlorite abundance or assigned wholly to H_2O evolution.

The small intermediate-temperature mass rise also requires caution. If oxygen was present, uptake associated with oxidation of Fe-bearing phases could partly offset concurrent volatile release. Instrumental baseline effects are another possible contribution at the small magnitude displayed. Without the purge-gas specification and baseline information, this feature cannot establish magnetite oxidation, sulfide oxidation or the formation of a particular product. Thermal studies of chalcopyrite

CC BY

REMUNOM
ISSN 2178-6925

Received: 10/11/2026 - **Accepted:** 15/11/2026
Vol: 13.24
DOI: 10.66104/vhwccn53
Pages: 1-24

demonstrate the importance of controlled heating conditions and complementary analysis of reaction products (Kizilca and Copur, 2016). The present dataset contains no evolved-gas identification or post-heating diffraction to separate these alternatives.

The DSC trace shows low-temperature structure, a broad downward feature near approximately 390 °C, a smaller feature around 430 °C and a sustained downward trend above approximately 470 °C. Because the figure defines exothermic direction upward, downward features are in the endothermic direction. Nevertheless, the long downward trajectory cannot be treated as a series of quantitatively separated reaction peaks without baseline treatment. Quartz undergoes an α–β transition near 573 °C, as established in experimental thermal studies (Breuer and Schilling, 2021), but a discrete transition peak cannot be confidently resolved in this composite trace. Its possible contribution must remain distinct from a claimed experimental identification at exactly 573 °C.

The approximately 2.3% TG loss and the 2.00 wt.% LOI are of similar magnitude. Their difference of roughly 0.3 percentage points is not sufficient to establish inconsistency, because endpoint mass losses depend on atmosphere, residence time, heating history and sample preparation. Conversely, agreement at this level does not validate an assignment to a single mineral. Oxidation-related mass gains can partly compensate for volatile losses in a material containing iron-bearing silicates, magnetite and chalcopyrite. The thermal results support a limited net mass change and an elevated-temperature transformation interval, while the phases responsible remain incompletely resolved.

The BSE micrographs provide the particle-scale context that bulk analyses cannot supply (Figure 5). The four fields contain angular to subangular particles with varied outlines and internal grey-level contrasts. Some particles appear comparatively uniform, while others contain bright inclusions, patches or irregular domains within a darker host. The lower-left field shows conspicuous adjoining regions of contrasting brightness within large particles, and the lower-right field includes elongated particles with smaller bright domains. These are qualitative observations of compositional heterogeneity and composite textures at the

CC BY

REMUNOM
ISSN 2178-6925

Received: 10/11/2026 - **Accepted:** 15/11/2026
Vol: 13.24
DOI: 10.66104/vhwccn53
Pages: 1-24

displayed scale.

Figure 5. Backscattered-electron micrographs of the copper ore obtained at 372× magnification and 20 kV, illustrating particle morphology, internal compositional contrasts, and mineral associations.

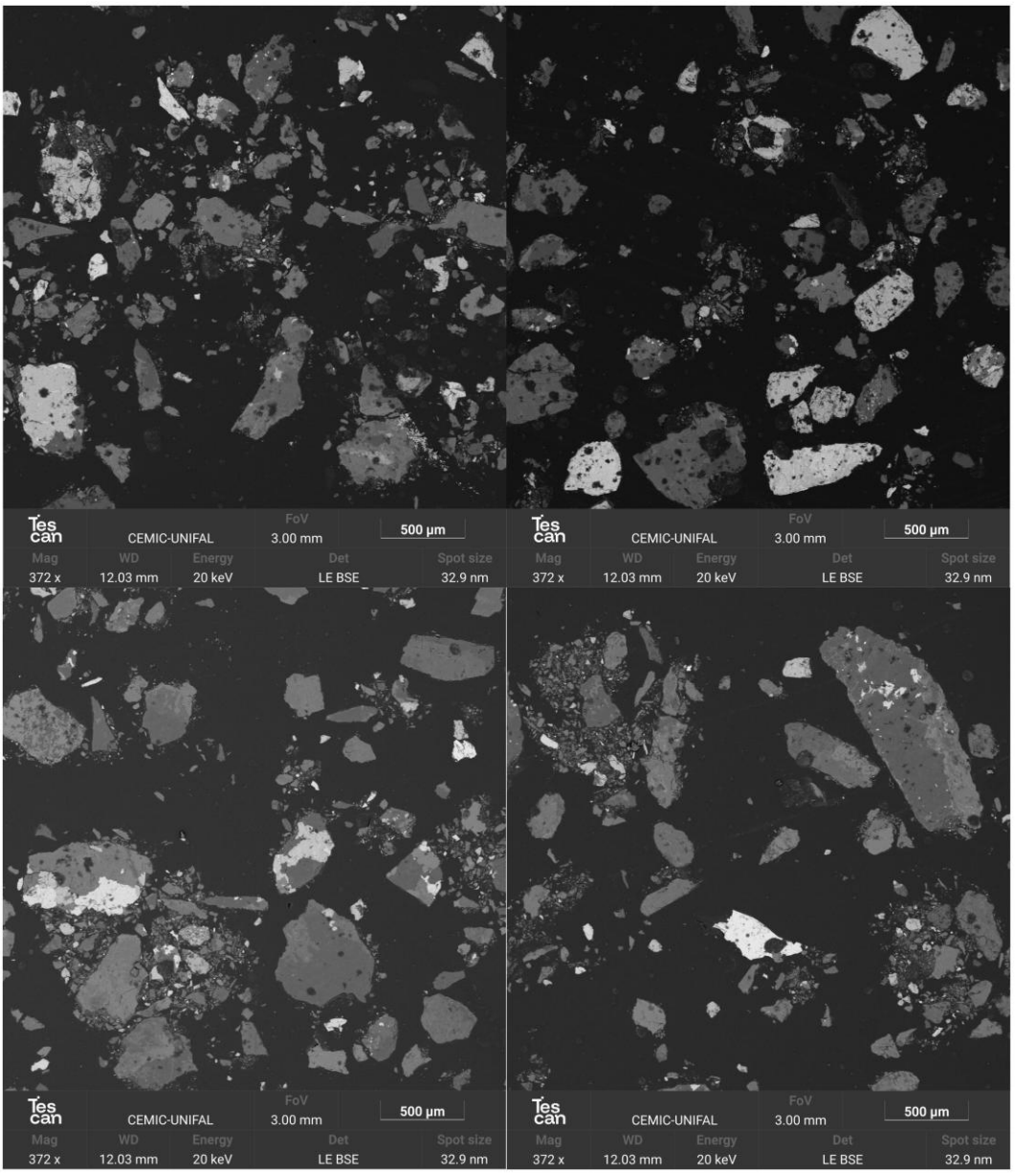

The brighter domains are consistent with a higher mean atomic-number response under comparable preparation and imaging conditions. In the context of the bulk assemblage, Fe- and Cu-bearing phases are plausible contributors, but the

CC BY

REMUNOM
ISSN 2178-6925

Received: 10/11/2026 - **Accepted:** 15/11/2026
Vol: 13.24
DOI: 10.66104/vhwccn53
Pages: 1-24

images do not distinguish magnetite from chalcopyrite on a particle-by-particle basis. Dark regions within particles may include lower-contrast minerals, voids or preparation-related features; the continuous dark background is consistent with mounting material. Without a preparation record and higher-resolution inspection, dark features should not be reported as quantified porosity or connected cracks. Likewise, nearby fine fragments in a polished field do not demonstrate aggregation in an aqueous suspension.

The micrographs establish that at least part of the material contains contrasting domains within common particle boundaries. They do not establish a copper liberation size or the fraction of fully liberated chalcopyrite. Fandrich et al. (2007) describe how mineral identification and image analysis must be combined for quantitative liberation assessment, while Zhang et al. (2021) illustrate the value of automated mineral liberation analysis in copper sulfide tailings. The present images support the existence of textural complexity, but a two-dimensional cut can expose an internal domain that remains enclosed within the three-dimensional particle.

The combined characterization results reveal a silicate-rich mineral assemblage containing chalcopyrite and magnetite, with iron also potentially hosted by chlorite and amphibole. FTIR and TG–DSC indicate the presence of hydrous constituents undergoing thermal transformations, while SEM reveals compositional contrasts within individual particles. These characteristics provide a basis for investigating copper exposure, gangue rejection, and the behavior of iron-bearing phases during mineral processing.

3.2 Implications for mineral processing

The first processing implication concerns the balance between exposing valuable minerals and generating unnecessary fines. The SEM fields show composite textures, while XRD identifies a mechanically heterogeneous assemblage. These observations justify investigating how mineral interfaces influence breakage, but they do not establish that the present ore is either easy or

CC BY

REMUNOM
ISSN 2178-6925

Received: 10/11/2026 - **Accepted:** 15/11/2026
Vol: 13.24
DOI: 10.66104/vhwccn53
Pages: 1-24

difficult to grind. Rincon et al. (2019) combined mineralogical information with measured comminution indices because the effect of texture depends on the actual loading response. For the present material, grinding investigations should distinguish bulk size reduction from increased exposure of the copper-bearing fraction.

A single target particle size cannot be inferred from the 500 μm SEM scale bars. A large composite particle may contain both coarse and much finer internal domains, and apparently isolated bright areas in a section may remain attached to other minerals outside that plane. A suitable liberation investigation would therefore examine successive size fractions, identify copper-bearing domains chemically and relate their exposure to metallurgical recovery. The objective would be to identify where additional grinding produces useful copper exposure and where it mainly fragments already liberated gangue. This distinction is relevant to the coexistence of substantial silicate content and a comparatively smaller copper-bearing fraction.

Studies of copper–cobalt ores provide useful methodological comparisons without implying equivalent mineralogy. Hu et al. (2021) showed that sulfide aggregates can be relevant units for primary flotation and tailings rejection, while Shi et al. (2025) used mineral associations in flotation products to guide circuit development. These findings suggest that complete separation of every constituent grain need not be imposed as the initial objective in a bulk sulfide recovery step. Whether analogous composite particles in this ore would be floatable depends on the amount and distribution of exposed chalcopyrite, which remain unmeasured.

Flotation is a justified candidate for experimental investigation because chalcopyrite is identified in the crystalline assemblage. The supporting evidence is the sulfide phase assignment, not the CuO reporting convention. However, the present characterization cannot specify collector type, reagent dosage, operating pH or the number of cleaning stages. Tijsseling et al. (2020) related flotation behavior to quantitative feed mineralogy across several ore samples, emphasizing that ore-specific information is needed to connect mineral occurrence with recovery. Here, initial flotation measurements would need to establish whether losses result chiefly from insufficient exposure, unfavorable surface conditions or hydraulic

CC BY

REMUNOM
ISSN 2178-6925

Received: 10/11/2026 - **Accepted:** 15/11/2026
Vol: 13.24
DOI: 10.66104/vhwccn53
Pages: 1-24

transport of fine material.

Chlorite deserves particular attention because it is supported by multiple low-angle diffraction features and is chemically consistent with the Mg, Al and Fe inventory. In chalcopyrite flotation systems, Pan et al. (2019) demonstrated selective depression of chlorite and serpentine by sodium alginate, including tests with real ore. This provides a specific example of how phyllosilicate control can improve selectivity. It does not establish sodium alginate as the optimum reagent for the present sample, and the serpentine component of that study must not be imported into the present mineral assemblage, where serpentine was not identified.

Control of chlorite must also distinguish surface hydrophobicity from entrainment. Chen et al. (2023) found that fine chlorite recovery was strongly affected by particle size and that high-molecular-weight carboxymethyl cellulose could reduce entrainment through flocculation. Their results show why a reagent that makes a gangue surface more hydrophilic may still provide insufficient rejection of very fine particles. For this ore, a decrease in concentrate MgO could reflect changes in either surface selectivity or water-associated transport. Measurements of water recovery and size-resolved gangue recovery would be required to separate these effects.

The amount of silica in the feed is not, by itself, evidence of severe rheological problems. Quartz is clearly identified, whereas amorphous silica has not been established. Chen et al. (2017) demonstrated that amorphous silica can alter pulp rheology and copper flotation in mixtures containing quartz and chalcopyrite, illustrating the need to distinguish silica forms. The present material may generate fine silicate particles during grinding, but neither a clay-size fraction nor a viscosity increase has been measured. A processing interpretation should therefore connect rheological concerns to measured fines and pulp behavior, instead of assigning them solely from SiO_2 or Al_2O_3 percentages.

Solution chemistry may further change the separation of chalcopyrite from silicates. Fornasiero and Ralston (2005) showed that Cu(II) and Ni(II) can activate quartz, lizardite and chlorite toward xanthate flotation under suitable conditions. Wang et al. (2022) investigated how calcium and ferric ions affect chalcopyrite

CC BY

REMUNOM
ISSN 2178-6925

Received: 10/11/2026 - **Accepted:** 15/11/2026
Vol: 13.24
DOI: 10.66104/vhwccn53
Pages: 1-24

depression by carboxymethyl cellulose. These findings make water composition and dissolved-metal release relevant variables for a silicate-rich ore containing Fe- and Cu-bearing phases. The bulk CaO and Fe_2O_3-equivalent values do not provide dissolved-ion concentrations, so any activation or depression mechanism would require direct solution measurements.

Magnetite introduces a possible magnetic separation contrast, but total iron content cannot be equated with a recoverable magnetite fraction. Some iron may occur in chlorite, amphibole and chalcopyrite. Moreover, the SEM images show composite particles, raising the possibility that a magnetic product could carry attached copper-bearing material or silicate gangue. Magnetic separation could be evaluated as a diagnostic fractionation step, provided that both products are assayed for copper and iron. Its placement before flotation cannot be justified from the present results because copper losses to a magnetic fraction have not been quantified.

For hydrometallurgy, the identification of chalcopyrite directs attention to dissolution conditions and accessibility. The assay corresponds to approximately 2.14 wt.% Cu, but that value does not indicate how much copper would dissolve in acid alone. Hernández et al. (2018) investigated chalcopyrite-bearing ore in acidified nitrate and saline media and demonstrated a strong dependence on solution conditions and temperature. Such evidence supports experimental evaluation of controlled oxidizing systems; it cannot be used to assign a copper extraction percentage to the present ore. Copper speciation, exposed sulfide surface and the state of reaction products would influence the result.

Gangue dissolution is a second hydrometallurgical constraint. The CaO and MgO contents sum to 10.67 wt.%, while Al_2O_3 adds 9.87 wt.%. Their mineral hosts determine whether and how rapidly they react with the leach solution. The detected assemblage includes plausible reactive silicates, so acid demand should be measured alongside copper extraction and dissolved Fe, Mg, Al and Ca. Thomas (2021) demonstrated the importance of including both dissolution and precipitation when interpreting gangue acid consumption. The present chemical data cannot be converted into a single stoichiometric acid requirement without knowing which

CC BY

REMUNOM
ISSN 2178-6925

Received: 10/11/2026 - **Accepted:** 15/11/2026
Vol: 13.24
DOI: 10.66104/vhwccn53
Pages: 1-24

mineral components react and the products formed.

An absence of labeled carbonate phases does not prove zero carbonate content, but it also does not justify treating the reported calcium as calcite. This distinction matters because assuming carbonate-hosted Ca would impose a different reaction mechanism and timescale from Ca hosted in feldspar, amphibole or apatite. Jumbo-Pacheco et al. (2025) examined how NaCl influences gangue dissolution and copper leaching kinetics in a low-grade copper ore, showing that the chemistry of the matrix can alter access to copper. For the present material, changes in gangue dissolution could be beneficial for exposure while also increasing reagent demand; both outcomes would need to be measured.

The thermal results identify an interval in which the material undergoes appreciable net mass change, but do not establish a beneficial thermal pretreatment. Dehydroxylation could alter hydrous silicate structures, while differential thermal expansion across interfaces could affect particle integrity. At the same time, heating in an oxidizing environment may modify sulfide surfaces or convert iron-bearing phases, with consequences for both flotation and magnetic response. The broad DSC trend and small TG mass rise cannot distinguish these outcomes. Thus, an apparent thermal event should not be interpreted as proof of enhanced liberation or improved copper recovery.

Microwave-assisted comminution studies illustrate the need to assess both structural change and downstream performance. Batchelor et al. (2016) demonstrated changes in liberation and flotation of a porphyry copper ore following microwave treatment, while Oliveira Cubi et al. (2026) examined combined microwave and ultrasound pretreatment in a polymetallic ore. These results concern tested materials and treatment conditions. In the present study, magnetite and chalcopyrite provide a mineralogical reason to consider differential heating, but dielectric properties, energy consumption, temperature gradients and treatment response were not measured. Conventional TG–DSC cannot supply these quantities or demonstrate an energy advantage.

Table 1 summarizes the main links between observed characteristics and processing questions. The evidence is strongest for the coexistence of silicate

CC BY

REMUNOM
ISSN 2178-6925

Received: 10/11/2026 - **Accepted:** 15/11/2026
Vol: 13.24
DOI: 10.66104/vhwccn53
Pages: 1-24

gangue, chalcopyrite and magnetite, and for visible particle-scale heterogeneity. The largest unresolved variables are copper deportment, three-dimensional exposure, fine-particle behavior and gangue reactivity under actual process conditions. Resolving those variables would determine whether a reduction in gangue mass, selective grinding, reagent control or a leaching strategy provides a measurable benefit for this ore.

Table 1. Main characteristics of the copper ore and their implications for subsequent mineral processing investigations.

Characteristic	**Experimental basis**	**Processing implication**
Silicate-rich chemistry and quartz–feldspar assemblage	49.23 wt.% SiO_2; quartz and feldspar reflections	Evaluate gangue rejection and grinding response; bulk silica does not define hardness or liberation size.
Chalcopyrite-bearing copper mineralization	Chalcopyrite assignment by XRD; 2.68 wt.% CuO equivalent	Test sulfide flotation and controlled leaching; quantify copper deportment and exposed surface.
Hydrous, Mg- and Al-bearing gangue	Chlorite/amphibole assignments; OH-related absorption; MgO and Al_2O_3	Examine chlorite entrainment, reagent selectivity and size-dependent gangue recovery.
Iron-bearing mineral assemblage	Magnetite reflections; 21.22 wt.% Fe_2O_3 equivalent	Measure magnetic response with copper accounting; total Fe is not a magnetite assay.
Composite particle textures	Contrasting domains within particle boundaries in BSE images	Determine mineral-specific exposure and liberation across size fractions.
Potentially reactive gangue	CaO + MgO = 10.67 wt.%; several possible mineral hosts	Measure acid consumption, gangue dissolution and precipitation together with Cu extraction.
Limited net thermal mass loss	Approximately 2.3% loss by 1000 °C; strongest decrease at elevated temperatures	If heating is tested, verify phase changes and separation response; thermal curves do not establish a process benefit.

CC BY

REMUNOM
ISSN 2178-6925

Received: 10/11/2026 - **Accepted:** 15/11/2026
Vol: 13.24
DOI: 10.66104/vhwccn53
Pages: 1-24

4. Conclusions

The copper ore presented a silicate-rich chemical composition, with 49.23 wt.% SiO_2, 21.22 wt.% Fe_2O_3 equivalent and 9.87 wt.% Al_2O_3. Its 2.68 wt.% CuO-equivalent content corresponds to approximately 2.14 wt.% elemental Cu on the same reporting basis. This conversion does not imply that copper occurs as an oxide mineral.

The qualitative XRD assemblage comprised quartz, chlorite, amphibole, feldspars, magnetite, chalcopyrite and apatite. The identified silicates provide plausible hosts for the major chemical components, while chalcopyrite establishes the presence of a copper-bearing sulfide. Mineral abundances and the proportion of total copper hosted by chalcopyrite were not quantified.

FTIR absorption in the silicate and OH-related regions supported the coexistence of framework silicates and hydrogen-bearing components. TG indicated approximately 2.3% net mass loss by 1000 °C, with the principal decrease at elevated temperatures. Hydrous mineral transformations are consistent with this behavior, but individual reactions and the quartz transition were not independently resolved from the composite thermal trace.

BSE images showed angular particles and contrasting domains within some particles, supporting textural heterogeneity without identifying individual phases or quantifying liberation. These observations make copper exposure and the distribution of composite particles central questions for subsequent comminution and concentration studies.

The integrated characterization identifies chlorite rejection and entrainment control as important considerations for flotation, while gangue dissolution and copper accessibility are relevant to leaching. The presence of magnetite also suggests the possibility of magnetic fractionation. These findings provide a mineralogical and microstructural basis for subsequent beneficiation studies.

CC BY

REMUNOM
ISSN 2178-6925

Received: 10/11/2026 - **Accepted:** 15/11/2026
Vol: 13.24
DOI: 10.66104/vhwccn53
Pages: 1-24

References

Batchelor, A.; Jones, D.; Plint, S.; Kingman, S. (2016). Increasing the grind size for effective liberation and flotation of a porphyry copper ore by microwave treatment. Minerals Engineering, 94, 61-75. https://doi.org/10.1016/j.mineng.2016.05.011

Breuer, S.; Schilling, F. R. (2021). Anisotropic thermal transport properties of quartz: from −120 °C through the α – β phase transition. European Journal of Mineralogy, 33(1), 23-38. https://doi.org/10.5194/ejm-33-23-2021

Che, C.; Glotch, T. D.; Bish, D. L.; Michalski, J. R.; Xu, W. (2011). Spectroscopic study of the dehydration and/or dehydroxylation of phyllosilicate and zeolite minerals. Journal of Geophysical Research, 116(E5), E05007. https://doi.org/10.1029/2010je003740

Chen, X.; Hadde, E.; Liu, S.; Peng, Y. (2017). The effect of amorphous silica on pulp rheology and copper flotation. Minerals Engineering, 113, 41-46. https://doi.org/10.1016/j.mineng.2017.08.001

Chen, Y.; Chen, Y.; Zhang, L. (2023). Effect of the Molecular Weight of Carboxymethyl Cellulose on the Flotation of Chlorite. Materials, 16(9), 3356. https://doi.org/10.3390/ma16093356

Dehaine, Q.; Tijsseling, L. T.; Rollinson, G. K.; Buxton, M. W. N.; Glass, H. J. (2022). Geometallurgical Characterisation with Portable FTIR: Application to Sediment-Hosted Cu-Co Ores. Minerals, 12(1), 15. https://doi.org/10.3390/min12010015

Fandrich, R.; Gu, Y.; Burrows, D.; Moeller, K. (2007). Modern SEM-based mineral liberation analysis. International Journal of Mineral Processing, 84(1-4), 310-320. https://doi.org/10.1016/j.minpro.2006.07.018

Fornasiero, D.; Ralston, J. (2005). Cu(II) and Ni(II) activation in the flotation of quartz, lizardite and chlorite. International Journal of Mineral Processing, 76(1-2), 75-81. https://doi.org/10.1016/j.minpro.2004.12.002

Gaweł, B. A.; Ulvensøen, A.; Łukaszuk, K.; Arstad, B.; Muggerud, A. M. F.; Erbe, A. (2020). Structural evolution of water and hydroxyl groups during thermal, mechanical and chemical treatment of high purity natural quartz. RSC Advances, 10(48), 29018-29030. https://doi.org/10.1039/d0ra05798c

Hernández, P. C.; Taboada, M. E.; Herreros, O. O.; Graber, T. A.; Ghorbani, Y. (2018). Leaching of Chalcopyrite in Acidified Nitrate Using Seawater-Based Media. Minerals, 8(6), 238. https://doi.org/10.3390/min8060238

CC BY

REMUNOM
ISSN 2178-6925

Received: 10/11/2026 - **Accepted:** 15/11/2026
Vol: 13.24
DOI: 10.66104/vhwccn53
Pages: 1-24

Hu, W.; Tian, K.; Zhang, Z.; Guo, J.; Liu, X.; Yu, H.; Wang, H. (2021). Flotation and Tailing Discarding of Copper Cobalt Sulfide Ores Based on the Process Mineralogy Characteristics. Minerals, 11(10), 1078. https://doi.org/10.3390/min11101078

Jumbo-Pacheco, P.; Townley, B.; Kelm, U.; Vargas, T. (2025). Chloride leaching of copper ores: influence of NaCl on gangue dissolution and its effect on copper leaching kinetics. Minerals Engineering, 233, 109640. https://doi.org/10.1016/j.mineng.2025.109640

Kizilca, M.; Copur, M. (2016). Investigation of the Thermal Decomposition Kinetics of Chalcopyrite Ore Concentrate using Thermogravimetric Data. Chemical Engineering Communications, 203(5), 692-704. https://doi.org/10.1080/00986445.2015.1056298

Lempart, M.; Derkowski, A.; Luberda-Durnaś, K.; Skiba, M.; Błachowski, A. (2018). Dehydrogenation and dehydroxylation as drivers of the thermal decomposition of Fe-chlorites. American Mineralogist, 103(11), 1837-1850. https://doi.org/10.2138/am-2018-6541

Lempart, M.; Derkowski, A.; Strączek, T.; Kapusta, C. (2020). Systematics of H2 and H2O evolved from chlorites during oxidative dehydrogenation. American Mineralogist, 105(6), 932-944. https://doi.org/10.2138/am-2020-7326

Oliveira Cubi, G. M.; dos Reis, V. C.; da Silva, F. L.; Lopes, M. S.; Oliveira Cubi, G. J. (2026). Ultrasound activation of microwave-induced damage for enhanced grindability and mineral liberation in a polymetallic ore. Minerals Engineering, 249, 110834. https://doi.org/10.1016/j.mineng.2026.110834

Pan, G.; Zhang, G.; Shi, Q.; Chen, W. (2019). The Effect of Sodium Alginate on Chlorite and Serpentine in Chalcopyrite Flotation. Minerals, 9(3), 196. https://doi.org/10.3390/min9030196

Prameena, B.; Anbalagan, G.; Gunasekaran, S.; Ramkumaar, G.; Gowtham, B. (2014). Structural, optical, electron paramagnetic, thermal and dielectric characterization of chalcopyrite. Spectrochimica Acta Part A: Molecular and Biomolecular Spectroscopy, 122, 348-355. https://doi.org/10.1016/j.saa.2013.10.065

Rincon, J.; Gaydardzhiev, S.; Stamenov, L. (2019). Coupling comminution indices and mineralogical features as an approach to a geometallurgical characterization of a copper ore. Minerals Engineering, 130, 57-66. https://doi.org/10.1016/j.mineng.2018.10.007

Shi, Y.; Wang, J.; Ba, H.; Liu, W.; Yang, Y.; Liu, X.; Chen, T.; Fang, C. (2025). Process-Mineralogy-Guided Flotation for Cu-Co Recovery: A Case Study of DRC Copper–Cobalt Sulfide Ore. Processes, 13(3), 918. https://doi.org/10.3390/pr13030918

CC BY

REMUNOM
ISSN 2178-6925

Received: 10/11/2026 - **Accepted:** 15/11/2026
Vol: 13.24
DOI: 10.66104/vhwccn53
Pages: 1-24

Thomas, M. (2021). Understanding gangue acid consumption in copper sulfide heap leaching: Predicting the impact of carbonates, silicates and secondary precipitates. Minerals Engineering, 171, 107090. https://doi.org/10.1016/j.mineng.2021.107090

Tijsseling, L. T.; Dehaine, Q.; Rollinson, G. K.; Glass, H. J. (2020). Mineralogical Prediction of Flotation Performance for a Sediment-Hosted Copper–Cobalt Sulphide Ore. Minerals, 10(5), 474. https://doi.org/10.3390/min10050474

Vaitkus, A.; Merkys, A.; Gražulis, S. (2021). Validation of the Crystallography Open Database using the Crystallographic Information Framework. Journal of Applied Crystallography, 54(2), 661-672. https://doi.org/10.1107/s1600576720016532

Wang, C.; Liu, R.; Zhai, Q.; Wu, M.; Jing, N.; Xie, F.; Sun, W. (2022). Influence of calcium and ferric ions on the depression of chalcopyrite by CMC: Flotation performance and adsorption mechanism study. Minerals Engineering, 184, 107667. https://doi.org/10.1016/j.mineng.2022.107667

Zhang, X.l.; Kou, J.; Sun, C.b.; Zhang, R.y.; Su, M.; Li, S.f. (2021). Mineralogical characterization of copper sulfide tailings using automated mineral liberation analysis: A case study of the Chambishi Copper Mine tailings. International Journal of Minerals, Metallurgy and Materials, 28(6), 944-955. https://doi.org/10.1007/s12613-020-2093-1

CC BY